Check for updates

New insights into the beneficial roles of dispersants in reducing negative influence of Mg^{2+} on molybdenite flotation

Yubiao Li, [iD] *[ab] Xu Yang,[a] Jiali Fu,[a] Wanqing Li[a] and Chenglong Hu[a]

Due to the shortage of freshwater, seawater has been widely considered for mineral flotation. However, the presence of Mg^{2+} in seawater plays an apparently negative role. In this work, two dispersants (*i.e.*, sodium silicate (SS) and sodium hexametaphosphate (SH)) were applied to reduce the detrimental effects of Mg^{2+} on the flotation of molybdenite (MoS$_2$). Various measurements including contact angle, zeta potential, FTIR and XPS were carried out to understand the impacts of these two dispersants on MoS$_2$ flotation. Results indicate that both dispersants prevented the adsorption of colloidal Mg(OH)$_2$ onto MoS$_2$ surface under alkaline conditions, thereby improving MoS$_2$ floatability. In addition, both dispersants are physically adsorbed on MoS$_2$ surface, but chemically adsorbed on Mg(OH)$_2$ surface. In addition, the extended Derjaguin–Landau–Verwey–Overbeek (DLVO) calculation suggests that both SS and SH reverse the total interaction energies between MoS$_2$ and colloidal Mg(OH)$_2$ from negative (attraction force) to positive (repulsive force), with the impact of SH being more significant.

1. Introduction

Molybdenite (MoS$_2$), as the most important molybdenum (Mo)-containing mineral,[1–3] is frequently associated with Cu-bearing minerals and concentrated *via* flotation which consumes a significant amount of water.[4,5] Generally, the quality of flotation media highly affects mineral flotation efficiency[6] while freshwater is normally considered as an ideal medium.[7] However, freshwater only accounts for about 0.5–0.8% of the total water source on Earth.[8] Therefore, there is an increasing demand in applying alternative water sources like seawater containing high concentrations of electrolytes to minimize the usage of freshwater.[9]

Previous studies show that bubble coalescence can be inhibited when the concentration of electrolytes in seawater (*e.g.*, NaCl, KCl, CaCl$_2$, MgCl$_2$ and MgSO$_4$) exceeds the threshold for critical coalescence.[10–12] However, seawater inhibits MoS$_2$ flotation under alkaline conditions, primarily due to the adsorption of colloidal Mg(OH)$_2$ precipitated onto MoS$_2$ surface.[13–15] Therefore, great efforts have been made to reduce the negative influence of seawater (especially Mg^{2+} ions). For instance, Suyantara, *et al.*[16] reported that the addition of emulsified kerosene prevented the adsorption of Mg(OH)$_2$ onto

MoS$_2$. Jeldres, *et al.*[17] found that the addition of Na$_2$CO$_3$ and CaO reduce Mg-hydroxyl complexes on MoS$_2$ surface, thus improving MoS$_2$ recovery.

In both industrial implementation and fundamental studies, sodium silicate (SS) and sodium hexametaphosphate (SH) are commonly used as dispersants to disperse hydrophilic substances from the surface of valuable minerals.[18–20] Recently, more attention has been paid to the effects of these dispersants on mineral flotation in seawater. For instance, our previous studies[21,22] have shown that the addition of SH can form dissolvable complexes with Mg^{2+}, reducing the generation and adsorption of hydrophilic complexes on mineral surfaces. Others have also reported that Mg^{2+} plays the most significantly negative role in reducing the floatability of minerals in seawater.[13,23] However, the influencing mechanisms of Mg^{2+} on MoS$_2$ flotation are still not fully understood when using SS or SH.

In this study, MoS$_2$ flotation was carried out in the solution containing Mg^{2+} ions in the presence of SS and SH, to investigate the influencing mechanisms of these two dispersants on MoS$_2$ flotation, with the assistance of various analyses such as contact angle, zeta potential, FTIR and XPS. Moreover, the interaction force between particles was predicted based on the Derjaguin–Landau–Verwey–Overbeek (EDLVO) theoretical calculation.

2. Materials and methods

2.1 Samples and reagents

The raw MoS$_2$ sample was purchased from Guilin, Guangxi province, China, which was crushed, milled and wet sieved to

[a]School of Resources and Environmental Engineering, Wuhan University of Technology, Wuhan 430070, Hubei, China. E-mail: Xu.Yang@whut.edu.cn; Jiali.Fu@whut.edu.cn; Wanqing.Li@whut.edu.cn; 2578399685@qq.com

[b]Hubei Key Laboratory of Mineral Resources Processing & Environment, Wuhan University of Technology, Wuhan, 430070, Hubei, China. E-mail: Yubiao.li@whut.edu.cn
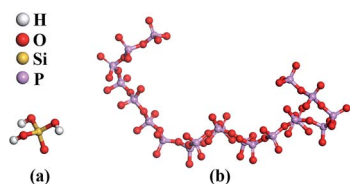
Fig. 1 The structures of SS (a) and SH (b).

a size fraction of 38–75 μm. This fraction of powder sample was then ultrasonically cleaned using ethanol to remove clinging fines. Subsequently, the sized MoS_2 was dried in a vacuum oven at 30 °C for 24 h, sealed with high purity N_2 in plastic tubes and then stored in a freezer to prevent oxidation. The elemental composition of the MoS_2 sample is given in our previous study,[21] indicating a high Mo concentration with a small portion of impurities.

0.1 M NaOH solution was used for pH adjustment. Analytical grade reagents including magnesium chloride hexahydrate ($MgCl_2 \cdot 6H_2O$), SS (Na_2SiO_3) and SH (($NaPO_3$)$_6$) were used. The structures of SS ($SiO(OH)_3^-$ as the main hydrolytic species) and SH (long-chain polymerized metaphosphate consisting of HPO_4^{2-}) were showed in Fig. 1, indicating totally different structures of these two dispersants. In addition, the Millipore® ultrapure water with a resistivity of 18.2 MΩ cm was used for solution preparation.

2.2 Flotation experiments

Laboratory flotation test was carried out using a mechanically agitated XFG II flotation machine (Wuhan Exploration Machinery Factory, China). Each solution suspension (25 mL) containing 0.25 g of sized MoS_2 and 0.05 M $MgCl_2$ (consistent with that of Mg^{2+} in seawater) was poured into the flotation cell (40 mL). When required, SS or SH was added into the pulp, followed by the addition of NaOH solution to maintain the desired pH (e.g., pH 10 to depress pyrite[24]) for 6 min, prior to flotation. The pulp was stirred at 1200 rpm with a constant airflow rate of 1.2 cm s^{-1}, while the froth product was collected at a time interval of 10 s. Both filtered froth products and residues were vacuum-dried at 30 °C for 24 h prior to weighing and recovery calculation. No collectors were applied to investigate the mechanisms of dispersants more clearly, i.e. excluding the influence from collectors.

2.3 Contact angle measurements

The fresh MoS_2 surface was obtained by peeling off the top layer of MoS_2 slab which was immersed into the conditioned solution same to the flotation experiment. The treated surface was then washed softly using ultrapure water and air-dried. 0.25 μL of ultrapure water was dropped onto the treated MoS_2 surface using a micro-syringe. Subsequently, the contact angle of MoS_2 was measured using a JC2000C device (Shanghai Zhongchen Digital Technology Company, China). The average values of triplicate measurements were reported herein.

2.4 Zeta potential measurements

Zeta potential of MoS_2 particles was determined via electrophoretic mobility analysis,[25] using a Nano-ZS90 zeta potential analyzer (Malvern Co., Ltd., UK), at room temperature. Prior to analysis, 50 mg of MoS_2 particles (<5 μm) were mixed in 50 mL solution for 10 min. The suspension pH was adjusted to desired value by adding NaOH solution. Finally, triplicate measurements were conducted and the average zeta potential value was reported.

2.5 FTIR measurements

50 mL of suspension (pH 10) containing 0.5 g of MoS_2 was stirred for 10 min. The filtered sample was washed using ultrapure water, and then freeze-dried under vacuum for 24 h. 2.5 mg of dried sample was mixed with KBr (250 mg) prior to pressing into thin pellets. The FTIR measurements were carried out using a Nicolet IS-10 instrument (Thermo Fisher Scientific Inc., Waltham, MA, USA).

2.6 XRD measurements

In addition to the MoS_2 sample, the precipitation formed in the solution was also sampled and analyzed by X-ray diffraction (XRD, D8 Advance, Bruker, Germany). Cu target and Kα ray were used as X-ray sources, the wavelength, tube voltage and tube current were controlled at 0.154056 nm, 40 kV and 30 mA in the test, respectively. Scanning speed and range were 3° min^{-1} and 10–70°, respectively. The XRD analysis indicated that the majority of this sample was well-crystallized MoS_2.

2.7 XPS measurements

The elemental concentration of surface chemical species on MoS_2 surface was determined by ESCALAB 250Xi XPS instrument (Thermo Fisher Scientific Inc., Waltham, MA, USA) with an Al Kα monochromatic X-ray source (1486.6 eV). The XPS spectra were obtained at a step size of 1.0 eV. The survey and high-resolution spectra were collected with pass energies of 100 eV and 30 eV, respectively. All XPS spectra data were analyzed using XPS Peak 4.1 software. Binding energy was calibrated based on C 1s at 284.8 eV.

2.8 EDLVO calculation

Extended Derjaguin–Landau–Verwey–Overbeek (EDLVO) theoretical model is used to predict the interaction energy between particles in aqueous, normally with van der Waals (V_W) and electrostatic interaction energies (V_E). Once external substances are added, steric hindrance interaction energy (V_{SR}) should be considered. Therefore, the total interaction energy (V_T) can be described using eqn (1).[26-28]

$$V_T = V_W + V_E + V_{SR} \tag{1}$$

V_W can be calculated according to eqn (2).

$$V_W = -\frac{A}{6H}\left(\frac{R_1 R_2}{R_1 + R_2}\right) \tag{2}$$

H (nm) represents the distance between particles. R_1 and R_2 refer to the average radius of heterogeneous particles. R_1 (33 μm) and R_2 (3.8 μm) are the average radius of MoS$_2$ and Mg(OH)$_2$ particles. A is the effective Hamaker constant calculated using eqn (3).

$$A = \left(\sqrt{A_{11}} - \sqrt{A_{33}} \right)\left(\sqrt{A_{22}} - \sqrt{A_{33}} \right) \quad (3)$$

where A_{11}, A_{22} and A_{33} are the Hamaker constants of MoS$_2$, Mg(OH)$_2$ and water, respectively. The Hamaker constants of MoS$_2$ (A_{11}) and Mg(OH)$_2$ particles (A_{22}) are 9.38×10^{-20} J and 1.62×10^{-20} J,[29,30] respectively. The Hamaker constant of water A_{33} is 3.7×10^{-20} J.[31]

The electrostatic interaction energy between MoS$_2$ and colloidal Mg(OH)$_2$ can be calculated using eqn (4).

$$V_E = \frac{\Pi \varepsilon_0 \varepsilon_r R_1 R_2}{R_1 + R_2}\left(\psi_1^2 + \psi_2^2 \right)$$

$$\left\{ \frac{2\psi_1 \psi_2}{\psi_1^2 + \psi_2^2} \ln \frac{1 + e^{-\kappa H}}{1 - e^{-\kappa H}} + \ln\left(1 - e^{-2\kappa H}\right) \right\} \quad (4)$$

where κ^{-1} represents the thickness of electric double layer (0.180 nm^{-1}),[32] ε_0 and ε_r are the vacuum and relative dielectric constants of the continuous phase, respectively, $\varepsilon_0 \varepsilon_r = 6.95 \times 10^{-10}$ C^2 (J^{-1} m).[26] ψ_1 and ψ_2 are the surface potentials of particles.[33]

As indicated in previous studies, the addition of SH results in steric hindrance interaction due to the steric hindrance effects.[26,28,34] Therefore, the steric hindrance interaction should be considered and can be calculated based on eqn (5).

$$V_{SR} = \frac{4\Pi R^2 \left(\delta - \frac{H}{2}\right)}{Z(R + \delta)} kT \ln\left(\frac{2\delta}{H}\right) \quad (5)$$

where k stands for the Boltzmann constant, 1.381×10^{-23} J K^{-1},[26] R is the radius of particles, δ represents the thickness of the adsorbed layer (5.45 nm (ref. 28)), and Z refers to the covering area of the macromolecules on the particle surfaces.

3. Results

3.1 Flotation results

Fig. 2a shows the MoS$_2$ recovery at 10 min as a function of dispersant (SS or SH) dosage from 0 to 50 mg L^{-1} in 0.05 M MgCl$_2$ solution. In the absence of SS or SH, a low MoS$_2$ recovery of 22% was observed, indicating a negative role of Mg^{2+} on MoS$_2$ flotation, probably due to the formation and adsorption of Mg(OH)$_2$ precipitates on MoS$_2$ surface.[13,15] With the increase of SS/SH dosage, MoS$_2$ recovery was increased to various degrees, indicating the beneficial roles of SS and SH on MoS$_2$ flotation, with the latter being more significant. Specifically, the MoS$_2$ recovery dramatically increased from 22% to 78% when SH was increased to 30 mg L^{-1}. Further increase in SH dosage to 50 mg L^{-1} only slightly increased the recovery. Differently, the MoS$_2$ recovery increased linearly from 22% to 62% when SS dosage was increased from 0 to 50 mg L^{-1}. It should be note that the MoS$_2$ recovery using SS was still lower than that using SH. Therefore, 50 mg L^{-1} was selected for further study.
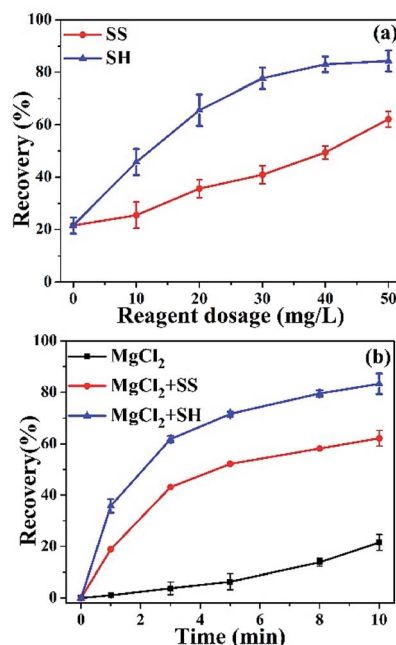

Fig. 2 Recovery of MoS$_2$ in 0.05 M MgCl$_2$ solution in the presence of SS or SH at pH 10. (a) Effect of dosage at 10 min, and (b) effect of flotation time.

Fig. 2b shows MoS$_2$ recovery as a function of time. In the absence of SS or SH, MoS$_2$ recovery was increased from 1% to 22% within 10 min, following an overall parabolic trend. However, MoS$_2$ recovery was increased more rapidly when dispersants were added, giving significantly greater recovery at 10 min, i.e., 62% and 83% in the presence of SS and SH, respectively.

3.2 Contact angle analysis

Fig. 3 shows the effect of SS/SH on the contact angle of MoS$_2$. The fresh MoS$_2$ surface shows a high contact angle of 87° in pure water (Fig. 3a), indicating a good hydrophobicity, similar to previous findings.[15,35] However, a contact angle of 71° was observed in 0.05 M MgCl$_2$ solution (Fig. 3b). When 50 mg L^{-1} of SS or SH was added, the contact angle of MoS$_2$ was increased to 80° (Fig. 3c) and 83° (Fig. 3d), respectively, suggesting that SS and SH increase the hydrophobicity of MoS$_2$ surface, with the effect of SH being more apparent on increasing contact angle of MoS$_2$.

3.3 Zeta potential analysis

Fig. 4 shows the zeta potentials of MoS$_2$ and Mg(OH)$_2$ with and without SS/SH at pH 10. The zeta potential of MoS$_2$ in the
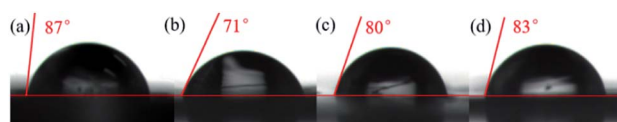

Fig. 3 Contact angles of MoS$_2$ in (a) pure water, (b) 0.05 M MgCl$_2$, (c) 0.05 M MgCl$_2$ with SS, and (d) 0.05 M MgCl$_2$ with SH, at pH 10.
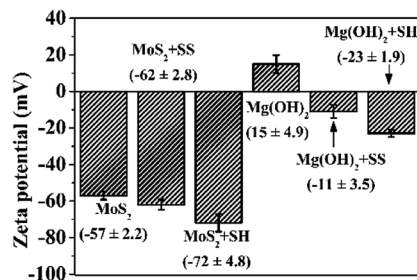
Fig. 4   Zeta potential of (a) MoS_2, (b) $Mg(OH)_2$ with and without SS/SH at pH 10.

Fig. 6   XPS survey spectra of untreated and treated MoS_2 in different solutions.

absence of SS or SH was -57 (±2.2) mV, close to that reported in Hirajima, *et al.*[5] However, this value was decreased to -62 (±2.8) mV and -72 (±4.8) mV, respectively, in the presence of SS or SH, indicating that SH plays a more significant role on decreasing the zeta potential of MoS_2.

However, $Mg(OH)_2$ surface was positively charged at pH 10, *i.e.*, 15 (±4.9) mV, consistent with that reported in Schott.[36] In the presence of SS/SH, the zeta potential of $Mg(OH)_2$ was decreased to -11 (±3.5) mV and -23 (±1.9) mV, respectively. The change of zeta potential of $Mg(OH)_2$ from positive (without SH or SS) to negative (with SH or SS) indicates the adsorption of negatively charged SH or SS on $Mg(OH)_2$ surface.[37,38]

3.4   FTIR analysis

FTIR spectral analyses (Fig. 5) were carried out to further understand the interaction between dispersants and colloidal $Mg(OH)_2$ or MoS_2 particles. The peak located at 881.8 cm^{-1} was assigned to P=O, while the peaks at 1019.3 and 1093.3 cm^{-1} were due to the stretching vibration of P–O.[26,39] The peak at 1274.7 cm^{-1} corresponds to the asymmetric stretching vibration of P–O–P.[28] The characteristic peaks at 631.9 cm^{-1} and
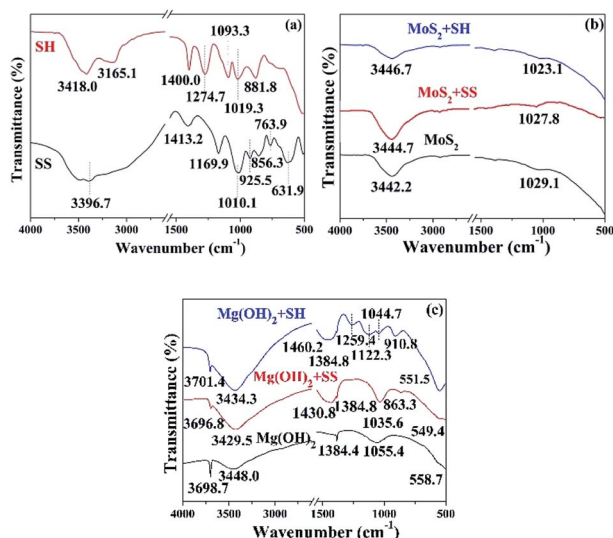
763.9 cm^{-1} for SS were attributed to the asymmetric deformation vibration of (H)O–Si–O(Na) and (H)O–Si–O(H), respectively. The peaks located at 856.3 cm^{-1} and 925.5 cm^{-1} were due to the symmetric stretching vibration of (Na)O–Si–O(H) and (Na)O–Si–O(Na), while the peaks at 1010.1 and 1169.9 cm^{-1} were ascribed to the asymmetric stretching vibration of Si–O(H) and Si–O(Na).[40] The characteristic peaks at 3300–3600 cm^{-1} were due to the stretching vibration of hydroxyl groups.[41,42]

Fig. 5b shows the spectra of MoS_2 with and without SH/SS. No new peaks appeared on MoS_2 in the presence of SH and SS, indicating that the adsorption of two dispersants on MoS_2 surface was dominated by physical adsorption. Fig. 5c shows the spectra of $Mg(OH)_2$ in the absence and presence of SH/SS. The sharp characteristic peaks at 1384.4 cm^{-1} and 3698.7 cm^{-1} were attributed to O–H vibrations of $Mg(OH)_2$.[43] The new characteristic peaks at 910.8, 1122.3, 1259.4 and 1460.2 cm^{-1} were due to the presence of SH on $Mg(OH)_2$ while the peaks at 910.8 and 1122.3 cm^{-1} were due to the shift of P=O peaks of SH at 881.8 and 1093.3 cm^{-1}, respectively. The characteristic peak at 1259.4 cm^{-1} was due to shift of P–O–P of SH that originally at 1274.7 cm^{-1}. Therefore, SH is chemically adsorbed on $Mg(OH)_2$. Similarly, new characteristic peaks at 1035.6 and 1430.8 cm^{-1} due to SS appeared on $Mg(OH)_2$ surface, indicating a chemical adsorption mechanism between SS and MoS_2.

3.5   XPS analysis

Fig. 6 shows the XPS survey for MoS_2 surfaces in the absence and presence of SH/SS. No characteristic peaks due to Mg 2s

Fig. 5   FTIR spectra of (a) SH and SS, (b) MoS_2, and (c) $Mg(OH)_2$ + SH/SS.

Table 1   Elemental quantification (at%) of untreated and treated MoS_2 surfaces

Element	BE (eV)	Conditions			
		Untreated	$MgCl_2$	$MgCl_2$+SS	$MgCl_2$+SH
S 2p	162.4	58	56	58	57
O 1s	533.2	7	10	7	7
Mo 3d	230.0	34	29	33	34
Mg 2s	89.5	1	5	2	2

Paper

were detected on the untreated MoS_2 surface, but appeared on MoS_2 surface treated in 0.05 M $MgCl_2$. The peak intensities of O 1s and C 1s were also increased significantly.

Table 1 shows that Mg 2s and O 1s were increased from 1 at% to 5 at% and 7 at% to 10 at%, respectively, indicating the adsorption of $Mg(OH)_2$ precipitates on MoS_2 surface in 0.05 M $MgCl_2$ solution.[34] However, upon addition of SH or SS, the peak intensities of Mg 2s and O 1s were reduced, e.g., from 5 at% to 2 at% and from 10 at% to 7 at%, respectively, indicating that the addition of these two dispersants can prevent the adsorption of $Mg(OH)_2$ precipitates on the surface of MoS_2.

4.   Discussion

Fig. 7 shows the XRD patterns of white precipitates formed in 0.05 M $MgCl_2$ solution. $Mg(OH)_2$ was found to be the predominant phase, with most crystal faces being detected, indicating a quick formation of crystalline $Mg(OH)_2$ under the flotation condition. As indicated in the previous studies[13–15] and Fig. 2 herein, MoS_2 flotation recovery was reduced in 0.05 M $MgCl_2$ solution, primarily due to the formation and adsorption of $Mg(OH)_2$ on MoS_2 surface, consistent with the contact angle measurements (Fig. 3). However, the mechanism between MoS_2 and $Mg(OH)_2$ is still not fully understood.

The dominant force between MoS_2 and $Mg(OH)_2$ can be calculated based on the EDLVO theory. Generally, the more negative V_T between particles, the greater the attraction force to aggregates. In contrast, the more positive V_T responds to the stronger repulsive force between particles, resulting in a more dispersed pulp system.[44,45] Fig. 8 shows that the V_T between MoS_2 and $Mg(OH)_2$ remains negative within the measured particle distance in the absence of dispersants, indicating the aggregation of MoS_2–$Mg(OH)_2$. In other words, $Mg(OH)_2$ is likely attached onto the MoS_2 surface in $MgCl_2$ solution in the absence of dispersants.

In the presence of SS, the V_T between MoS_2 and $Mg(OH)_2$ is gradually increased from a negative to a positive value when the distance increases, indicating that MoS_2 and $Mg(OH)_2$ particles repel each other.[46,47] Moreover, the V_T value between MoS_2 and $Mg(OH)_2$ in the presence of SH is always positive within the range of distance examined, suggesting a predominate repulsive force due to its long chain structure. As the adsorption of $Mg(OH)_2$ on MoS_2 surface decreases, the surface of MoS_2 becomes more hydrophobic, giving rise to the increase of MoS_2
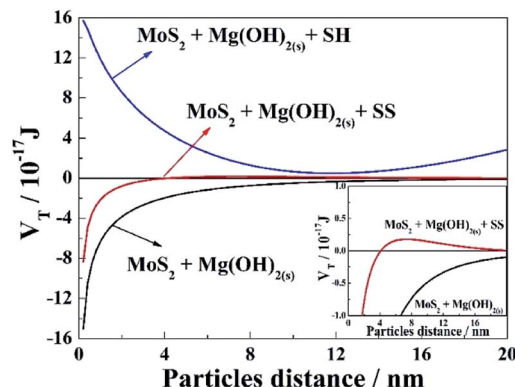

Fig. 8   Interaction energy between MoS_2 particles and $Mg(OH)_2$.

flotation that observed in Fig. 2. Therefore, SS and SH increase the repulsion between MoS_2 and $Mg(OH)_2$ particles, thereby decreasing the adsorption of $Mg(OH)_2$ on MoS_2 surface, with the effect of SH being more significant.

5.   Conclusions

A low recovery of 22% was found for MoS_2 flotation in 0.05 M $MgCl_2$ solution controlled at pH 10. MoS_2 recovery was increased significantly in the presence of SS/SH. Various measurements indicate that SS and SH were chemically adsorbed onto $Mg(OH)_2$, reversing its zeta potential from positive to negative. However, SS and SH were physically adsorbed onto MoS_2, further decreasing the zeta potential of MoS_2. The presence of SS and SH inhibits the adsorption of $Mg(OH)_2$ precipitates onto the negatively charged MoS_2 surface via electrostatic repulsion, thereby increasing MoS_2 recovery in 0.05 M $MgCl_2$. Further theoretical calculation demonstrates that the addition of SS or SH changes the interaction force between particles from attractive to repulsive, thereby preventing the adsorption of hydrophilic colloidal $Mg(OH)_2$ on the MoS_2 surface, with the influence of SH being more significant.

Conflicts of interest

There are no conflicts to declare.

Acknowledgements

Fig. 7   XRD patterns of precipitates formed in 0.05 M $MgCl_2$ solution.

References

1 S. Castro, A. Lopez Valdivieso and J. S. Laskowski, Int. J. Miner. Process., 2016, 148, 48–58.

2 Z. L. Wei and Y. B. Li, *Conservation and Utilization of Mineral Resources*, 2018, 31–36.

3 X. Zhang, F. F. Jia, B. Q. Yang and S. X. Song, *J. Phys. Chem.*, 2017, **121**, 9938–9943.

4 Z. G. Yin, W. Sun, Y. H. Hu, Q. J. Guan, C. H. Zhang, Y. S. Gao and J. H. Zhai, *Trans. Nonferrous Met. Soc. China*, 2017, 883–890.

5 T. Hirajima, M. Mori, O. Ichikawa, K. Sasaki, H. Miki, M. Farahat and M. Sawada, *Miner. Eng.*, 2014, **66–68**, 102–111.

6 S. Castro and J. S. Laskowski, *KONA Powder Part. J.*, 2011, 4–15.

7 W. Y. Liu, C. J. Moran and S. Vink, *Miner. Eng.*, 2013, **53**, 91–100.

8 L. F. Greenlee, D. F. Lawler, B. D. Freeman, B. Marrot and P. Moulin, *Water Res.*, 2009, **43**, 2317–2348.

9 B. Wang and Y. Peng, *Miner. Eng.*, 2014, **66–68**, 13–24.

10 J. J. Quinn, J. M. Sovechles, J. A. Finch and K. E. Waters, *Miner. Eng.*, 2014, **58**, 1–6.

11 R. M. Pashley, B. W. Ninham and V. S. J. Craig, *Nature*, 1993, **364**, 317–319.

12 R. R. Lessard and S. A. Zieminski, *Ind. Eng. Chem. Res.*, 1971, **10**, 260–269.

13 Z. H. Qiu, Q. X. Liu, G. Y. Liu and H. Zhong, *Colloids Surf., A*, 2016, **509**, 123–129.

14 T. Hirajima, G. P. W. Suyantara, O. Ichikawa, A. M. Elmahdy, H. Miki and K. Sasaki, *Miner. Eng.*, 2016, **96–97**, 83–93.

15 Y. B. Li, C. Lartey, S. X. Song, Y. J. Li and A. R. Gerson, *RSC Adv.*, 2018, **8**, 23364–23371.

16 G. P. W. Suyantara, T. Hirajima, A. M. Elmahdy, H. Miki and K. Sasaki, *Colloids Surf., A*, 2016, **501**, 98–113.

17 R. I. Jeldres, M. P. Arancibia Bravo, A. Reyes, C. E. Aguirre, L. Cortes and L. A. Cisternas, *Miner. Eng.*, 2017, **109**, 10–13.

18 E. Rebolledo, J. S. Laskowski, L. Gutierrez and S. Castro, *Miner. Eng.*, 2017, **100**, 71–74.

19 K. I. Marinakis and H. L. Shergold, *Int. J. Miner. Process.*, 1985, **14**, 177–193.

20 A. Ramirez, A. Rojas, L. Gutierrez and J. S. Laskowski, *Miner. Eng.*, 2018, **125**, 10–14.

21 W. Q. Li, Y. B. Li, Z. L. Wei, Q. Xiao and S. X. Song, *Minerals*, 2018, **8**, 17.

22 W. Q. Li, Y. B. A. Li, Q. Xiao, Z. L. Wei and S. X. Song, *Minerals*, 2018, **8**, 18.

23 Y. B. Li, W. Q. Li, Q. Xiao, N. He, Z. J. Ren, C. Lartey and A. R. Gerson, *Minerals*, 2017, **7**, 10.

24 Y. F. Mu, Y. J. Peng and R. A. Lauten, *Miner. Eng.*, 2016, **96–97**, 143–156.

25 M. R. Gittings and D. A. Saville, *Colloids Surf., A*, 1998, **141**, 111–117.

26 Y. P. Lu, M. Q. Zhang, Q. M. Feng, T. Long, L. M. Ou and G. F. Zhang, *Trans. Nonferrous Met. Soc. China*, 2011, **21**, 208–213.

27 M. Q. Zhang, J. T. Liu and Y. T. Wang, *J. China Coal Soc.*, 2008, **33**, 1058–1062.

28 Y. H. Wang, X. H. Chen, Y. M. Hu and Y. D. Lan, *J. Cent. South Univ.*, 2007, **38**, 238–244.

29 G. Zhang, Y. Zhang and S. Bao, *Minerals*, 2018, **8**, 18.

30 J. Ren, J. Shen and S. Lu, *Particle Dispersion Science and Technology*, Chemical Industry Press, Beijing, 2005.

31 C. J. V. Oss, R. F. Giese and P. M. Costanzo, *Clays Clay Miner.*, 1990, **38**, 151–159.

32 B. Feng, Y. P. Lu, Q. M. Feng and H. Li, *Ind. Eng. Chem. Res.*, 2012, **51**, 12089–12094.

33 T. Missana and A. Adell, *J. Colloid Interface Sci.*, 2000, **230**, 150–156.

34 W. Li and Y. Li, *Miner. Eng.*, 2019, **134**, 269–274.

35 S. Kelebek, *J. Colloid Interface Sci.*, 1988, **124**, 504–514.

36 H. Schott, *J. Pharm. Sci.*, 1981, **70**, 486–489.

37 W. A. Huang, Q. Lan, Z. S. Qiu, Y. Zhang, H. Y. Zhong and G. T. Feng, *Silicon*, 2016, **8**, 111–122.

38 Y. Ji, J. Wang and L. Xiang, *Mater. Res. Innovations*, 2015, **19**(S2), 147–151.

39 Q. M. Feng, Q. B. Zhou, G. F. Zhang, Y. P. Lu and S. Y. Yang, *Chin. J. of Nonferrous Met.*, 2011, **21**, 436–441.

40 I. Halasz, M. Agarwal, R. Li and N. Miller, *Catal. Lett.*, 2007, **117**, 34–42.

41 C. S. Xue, *Semicond. Photonics Technol.*, 2007, **13**, 222–224.

42 T. Bezrodna, G. Puchkovska, V. Shymanovska, J. Baran and H. Ratajczak, *J. Mol. Struct.*, 2004, **700**, 175–181.

43 L. R. Chang, F. H. Cao, J. S. Cai, W. J. Liu, J. Q. Zhang and C. N. Cao, *Electrochem. Commun.*, 2009, **11**, 2245–2248.

44 Q. Q. Lin, G. H. Gu, H. Wang, Y. C. Liu, J. G. Fu and C. Q. Wang, *Int. J. Miner., Metall. Mater.*, 2018, **25**, 1–10.

45 Z. Adamczyk and P. Weroński, *Adv. Colloid Interface Sci.*, 1999, **83**, 137–226.

46 W. Z. Yin and J. Z. Wang, *Trans. Nonferrous Met. Soc. China*, 2014, **24**, 3682–3687.

47 A. Liu, M. Q. Fan, Z. H. Li and J. C. Fan, *Int. J. Miner. Process.*, 2017, **168**, 1–8.